Article

Enhanced Intrinsic Activity and Stability of Au-Rh Bimetallic Nanostructures as Supportless Cathode Electrocatalyst for Oxygen Reduction in Alkaline Fuel Cells

Narayanamoorthy Bhuvanendran, Subramanian Balaji, Sita Cordelia, Sivakumar Pasupathi, Eswaramoorthy Muthusamy, and Il-Shik Moon

ACS Sustainable Chem. Eng., **Just Accepted Manuscript** • DOI: 10.1021/acssuschemeng.6b01257 • Publication Date (Web): 12 Oct 2016

Enhanced Intrinsic Activity and Stability of Au-Rh Bimetallic Nanostructures as Supportless Cathode Electrocatalyst for Oxygen Reduction in Alkaline Fuel Cells

B. Narayanamoorthy[b,c], S. Balaji[a,c], C. Sita[c], P. Sivakumar[c] M. Eswaramoorthy[d] and Il-Shik Moon[a]

[a]Department of Chemical Engineering, Sunchon National University, # 315 Maegok Dong, Suncheon 540-742, Chonnam, South Korea.

[b]Department of Chemistry, Faculty of Science, Sri Chandrasekharendra Saraswathi Viswa Mahavidyalaya (SCSVMV University), Enathur, Kanchipuram - 631 561, India.

[c]HySA Systems Competence Centre, South African Institute for Advanced Materials Chemistry, University of the Western Cape, Private BagX17, Bellville 7535, South Africa.

[d]Nanomaterials and Catalysis Lab, Chemistry and Physics of Materials Unit, Jawaharlal Nehru Centre for Advanced Scientific Research (JNCASR), Bangalore – 560 064, India.

Corresponding Author

Prof. Il-Shik Moon
E-mail: ismoon@sunchon.ac.kr
Fax: +82 61 750 3581; Tel: +82 61 750 3581

Abstract

The electroreduction of dioxygen on supportless Au-Rh bimetallic nanostructures (Au-Rh NC) synthesized by a surfactant template-free, single step chemical reduction method occurred with high intrinsic activity in an alkaline medium. Cyclic voltammetry and linear scan voltammetry together with X-ray diffraction and high-resolution electron microscopy showed that the improved performance of the Au-Rh NC towards dioxygen reduction could be due to the synergistic electronic effects of nano-bimetallic combination and its cluster-like morphology. The electrochemically active surface area (ECSA) was estimated to be 37.2 m^2 g^{-1} for supportless Au-Rh NC with a 3:1 atomic composition, which was higher than that reported for Ag-based nanocatalysts. The intrinsic activities (IA) of the supportless and carbon supported Au-Rh (3:1) NCs were 3.25 and 3.0 mA/cm^2, respectively, which were higher than those of the standard Pt/C (0.1 mA/cm^2)[45] Au/C catalysts for the oxygen reduction reaction (ORR). Oxygen reduction on both catalysts followed a direct four electron pathway. The accelerated durability test carried out by continuous potential cycling showed that the 3:1 ratio of Au-Rh nanostructures had excellent stability with a 20% increase in ECSA after 10000 potential cycles, highlighting their potential application for real systems.

Keywords: *Au-Rh; supportless electrocatalyst; durability; oxygen reduction; KOH.*

Introduction

The development of highly active cathode catalysts to catalyze the kinetically sluggish oxygen reduction reaction (ORR) is indispensable for making fuel cell technology cost effective.[1] Until now, Pt and Pt-based electrocatalysts were the prime choice for the ORR and have been studied extensively because of their superior electrocatalytic activity and life-time for low temperature fuel cells.[2-6] In particular, for alkaline fuel cells, a number of studies have focused on finding more efficient electrocatalysts with better activity and stability to replace the expensive and less abundant Pt.[6] Recently, Au and Ag-based electrocatalysts have attracted increasing attention as cathode catalyst materials for the ORR because of their higher efficiency in alkaline media.[7] Pure Au is generally considered a poor catalyst towards ORR due to the weak chemisorption properties caused by the filled d-band level.[8, 9] Although the use of Ag could reduce the cost of the catalysts, Au is the choice in terms of the onset potential for the ORR in alkaline medium because Au exhibits a more positive potential (i.e. lower over-potential) than Ag and is preferred for investigating the ORR.[10]

Au has attracted considerable research attention for the development of active catalysts towards electrochemical energy conversion systems.[11, 12] In recent years, many studies have examined the electrocatalytic performance of Au nanocatalysts for fuel cell reactions with particular emphasis on various nanomorphologies. Kuai et al. reported the preparation of Au icosahedra by PVP-stabilized hydrothermal synthesis at 120 °C. They reported that the Au icosahedra exhibited a lower overpotential than commercial Pt/C electrocatalyst and possessed ~ 1.6 fold higher limiting reduction current than the sphere-like Au nanoparticles.[13] Manivannan et al. synthesized raspberry-like Au nanostructures by electrodeposition and obtained good ORR activity with an onset potential of -0.06 V vs. Ag/AgCl and a mass activity of 31.7 mA/mg.[14] Yin et al. reported the facile synthesis of surfactant-free Au clusters on graphene sheets using a freeze

drying method and observed good oxygen reduction activity with an onset potential of -0.10 V in an alkaline medium.[15]

In general, the catalyst active sites are having an optimal adsorption of oxide species (O or OH) and thus playing an important role on catalyst surface poisoning. The surface reaction could not occur, if it is too weak, rather the strong adsorption of oxide species leads to the surface poisoning[16]. Based on the reported theoretical (DFT studies) and experimental investigations, it was clearly described that the activity of the monometallic nanoparticles could be further enhanced through the insertion of secondary metals which can alter the metal-metal bond distance and may increase the electronic (or) ligand effects referred to as the 'heterometallic bonding interactions'.[17] To improve the electrocatalytic activity of Au, many researchers have synthesized different nano architectures by alloying Au with secondary metals, such as Pt, Pd and Ag, which could increase the catalytic activity via a synergetic effect.[10, 11, 15-18] Jalili et al. predicted that the presence of a second metal could alter the adsorption energy of oxygen reduction intermediates (hydroxyl ion) on the Au surface by shifting the d-band center due to lattice strain and ligand effects.[18] Maye et al. demonstrated the synthesis of Au and AuPt electrocatalysts by encapsulation method using decanethiol and found higher specific mass activities of 1744 $mA/cm^2/mg_{metal}$ and 1147 $mA/cm^2/mg_{metal}$ for Au/C and AuPt/C electrocatalysts, respectively, in KOH medium.[19] Several Au based electrocatalysts were employed as cathode catalysts, including Au-Pt[12], Au-Pd[13] and Au-Ag[20] with different support materials[21, 22] and nanostructures.[23-25]

Among the platinum group metals, Rh has a good catalytic activity for a variety of heterogeneous reactions, such as hydrogenation, hydroformylation and hydrocarbonylation.[26] An oxophilic nature of Rh is playing a vital role as secondary element with Pt, Pd, Ag and Au catalysts for surface regeneration of active sites during fuel cell reactions. From the detailed

literature survey we found that although Rh by itself is not catalytically active, the influence of Rh nanoparticles on the catalytic activity with Pt was employed for both oxidation of small organic molecules and enhance the stability towards ORR.[27-29] Many reports have examined Rh-based catalysts for fuel cell reactions of both anodic (methanol and ethanol) oxidation.[29-31] and cathodic oxygen reduction.[32, 33] Compared to Pt, improved catalytic activity and durability was reported for ORR due to the synergistic effects between Pt and Rh.[35, 37] Therefore, the bimetallic nanostructure of Au-Rh, as an active electrocatalyst for the cathode half-cell reaction in alkaline medium, requires further investigation. In this study, supportless Au-Rh nanostructures (Au-Rh NC) were prepared by single step, green chemical reduction method using formic acid as the reducing agent without a template or surfactant. The shape, size and composition of the Au-Rh NC were analyzed by X-ray diffraction (XRD), scanning electron microscopy (SEM) and transmission electron microscopy (TEM). The electrocatalytic activity of supportless Au-Rh NC was evaluated for a range of compositions and also compared with Vulcan carbon (VC)-supported Au-Rh (Au-Rh/VC). The long-term stability of the supportless and carbon supported Au-Rh catalysts was examined by accelerated durability tests (ADT). The electrochemical and kinetics parameters are presented and discussed.

Material and Methods

Materials

Chloroauric acid ($HAuCl_4.6H_2O$), rhodium (III) chloride monohydrate ($RhCl_3.H_2O$) and formic acid (98 %) were obtained from Sigma-Aldrich. Vulcan carbon XC-72 was used (Cabot India Ltd) for the synthesis of carbon-supported catalysts. Nafion perfluorinated polymer resin solution (5 wt. %, Sigma-Aldrich) was used as a catalyst binder. Potassium hydroxide (Rankem),

methanol (98%, Merck) and absolute ethanol (Merck) were used as received. All solutions were prepared using Millipore (18 MΩ cm) water.

Synthesis of Au-Rh nanostructures

The supportless and carbon-supported Au-Rh NCs were synthesized using a single step chemical reduction procedure. Aqueous solutions of 15.4 mg of $HAuCl_4.6H_2O$ and 6 mg of $RhCl_3.H_2O$ both dissolved in 20 ml water were mixed with 1 ml of formic acid (1.2 M) drop-wise with stirring. The metal composition between Au and Rh was maintained at 3:1 based on the individual atomic weight percentages (after several trials on composition optimization). The final mixture was left to stand for 72 h at room temperature. A yellow to dark brown color change was observed 1 h after adding the reducing agent, which then turned to a black precipitate. After 72 h, the sample was collected by centrifugation, and washed several times with water and methanol. The final product obtained was dried in an air oven at 60 °C for 4 h. An appropriate amount of metal precursors were taken for different elemental compositions. For the carbon-supported catalysts, the same procedure was repeated using 7.5 mg of Vulcan carbon XC-72 (VC), which was added at the initial stage of the synthesis procedure before adding the reducing agent.

Physical characterization

Powder XRD (Bruker-D8) patterns were obtained using Cu-K_α radiation (λ=1.54 Å, step size: 0.02, current: 30 mA and voltage: 40 kV). The elemental composition of the catalyst was determined by an inductively coupled plasma-atomic emission spectrometer (ICP-AES, Thermo Electron IRIS INTREPID II XSP DUO) and energy-dispersive X-ray spectroscopy (EDS). Field-emission SEM (FESEM, FEI (Nova-Nano SEM-600, Netherlands) images were obtained. TEM (FEI Tecnai 30G2) images were obtained at an accelerating voltage of 300 kV.

Electrochemical characterizations

The catalyst-coated glassy carbon-rotating disc electrode (GC-RDE) was prepared by dispersing 0.5 mg of the catalyst in 1 ml of absolute ethanol and ultrasonicating for 3 min to obtain a homogeneous dispersion. A 7 µl sample of this prepared catalyst ink (slurry) was drop casted onto a mirror finished RDE-GC (metal loading of 17.8 µg/cm^2) substrate and covered by drop casting with 5 µl of Nafion solution (0.5 wt.%). Initially, the catalyst-coated electrode was subjected to potential cycling (25 scans) in a N_2 saturated 0.5 M KOH solution at a sweep rate of 0.1 V/s between -0.8 to 0.6 V vs. RHE at 25 °C. The actual cyclic voltammograms (CV) were recorded under similar conditions. The polarization curves (LSV) were recorded in an O_2-saturated electrolyte at a scan rate of 0.01 V/s at different electrode rotation rates of 400-2400 rpm. All potential values reported were referenced to the reversible hydrogen electrode (RHE). The stability of the Au-Rh electrocatalysts were examined by ADT by continuous potential cycling between -0.6 and +0.2 V in an O_2-saturated electrolyte at 0.1 V/s and measuring the CV and LSV patterns at regular intervals.

Results and discussion

Surface morphology of the Au-Rh nanostructures

From the powder XRD patterns, well-defined polycrystalline peaks were observed for both supportless and carbon-supported Au-Rh NC, as given in **Fig. 1**. All XRD peaks clearly showed that the Au-Rh NC consist of a face centered cubic (fcc) crystalline structure. The strong XRD peaks at 2θ values 38.9° and 39.6° for the supportless and carbon-supported Au-Rh NC, respectively, were attributed to the fcc crystalline plane of (111), which lies intermediate between the XRD peaks of the pure Au (111) at 38.1°[37] and Rh (111) at 41.1°.[38] This clearly shows the alloy formation between Au and Rh. In the carbon-supported Au-Rh catalyst, a broad

peak at 24.7° confirmed the presence of graphitic carbon.[23] Using the Scherrer equation, the mean crystallite size, which was calculated from the full width at half maximum of the (111) crystalline plane, was found to be 11.5 nm and 3.8 nm for the Au-Rh (3:1) NC and Au-Rh (3:1)/VC, respectively. FESEM revealed the supportless Au-Rh to be an aggregate of fairly dense, tiny nanoparticles with cluster morphology (*Supporting Information,* **Figs. S1a and S1b**), possibly due to the intermetallic stabilization and cohesive action and the EDS revealed an Au-Rh elemental composition of 74.2 % and 23.8 %, respectively, confirming the stoichiometric ratio of 3:1 (*Supporting Information,* **Fig. S2**). In addition to that the ICP-AES analyses were performed for Au-Rh catalyst and found to be the Au is around 72.9% and Rh is 22.1which is near to the EDX results and hence it is confirmed that the composition of Au and Rh is 3:1. **Figs. 2a and 2c** show TEM images of the Au-Rh (3:1) NC catalyst. The cluster morphology was confirmed by the uniform distribution of dark and light spots, indicating homogeneity between Au and Rh. In contrast, carbon-supported Au-Rh (3:1) NC showed a uniform distribution of spherical nanoparticles on a carbon substrate (**Figs. 2b and 2d**) and the mean particle size was determined from the corresponding histograms shown in **Figs. 2e and 2f**. The particle sizes were 10-12 nm for Au-Rh (3:1) and 3-4 nm for Au-Rh (3:1)/VC. The particle sizes obtained from XRD and TEM were almost similar. The high resolution-TEM image of supportless Au-Rh catalyst (inset of Fig. 2a) shows neat crystalline fringes with the lattice space of 0.21 nm corresponds to the (111) crystalline plane and it's not that much defined in the Au-Rh/VC catalyst (inset of Fig. 2b) and it's well correlated with the intensity of XRD peaks.

Au-Rh composition optimization

The Au-Rh atomic ratio was optimized based on the electrochemical performance of the electrocatalysts towards ORR from voltammetry studies. **Fig. S3a** (*Supporting Information*)

presents typical CVs of Au-Rh NC with different compositions recorded in a N_2 purged 0.5 M KOH solution at a scan rate of 0.1 V/s at 25 °C. The electrochemically active surface area (ECSA) of Au-Rh was determined from the oxide reduction peak due to the lack of hydrogen adsorption on the Au surface, which can be calculated using the following equation.[39, 40]:

$$ECSA = \frac{Q_O}{(Q_{ref} \times m)}$$

where Q_0 is the total charge for the oxide-reduction peak during the cathodic potential sweep ($\mu C/cm^2$), m is the metal loading ($\mu g/cm^2$) over the GC electrode and Q_{ref} is the charge required for the monolayer adsorption of oxygen on the Au surface (386 $\mu C/cm^2$).[3, 40] CV revealed a well-defined metal-oxide reduction peak only for Au-Rh (3:1) with a higher peak current density of ~7.5 mA/cm^2 (*Supporting Information,* **Fig. S3a**). In addition, a higher ECSA was obtained for Au-Rh (3:1) NC (32.7 m^2/g) than the other compositions investigated and also comparable to that reported for Au electrocatalysts.[40, 41]

The ORR activity of Au-Rh NC was probed by linear scan voltammetry (LSV) under an O_2 saturated 0.5 M KOH solution under hydrodynamic conditions (*Supporting Information,* **Fig. S3b**). Compared to the other catalysts, Au-Rh NCs (3:1) possessed a higher limiting current density of 4.41 mA/cm^2 with an earlier onset potential (-0.08 V). A well-defined Au-O(H) reduction peak was obtained at a higher potential region for Au-Rh (3:1) NC, whereas for a 1:1 composition, a broad peak was observed that almost disappeared at 1:3 composition ratio. This shows that the impact of the Au-Rh composition for ORR depends mainly on the Au content and the role of Rh might be to stabilize the cluster morphology. From the hydrodynamic polarization curves, the Koutecky-Levich (K-L) plots were constructed to calculate the number of electrons transferred (n) during the ORR.[44] The 'n' was found to be 4.1 for Au-Rh (3:1) NC and 3.6 and 2.4 for the (1:1) and (1:3) compositions, respectively. This confirms that the Au-Rh (3:1) NC

follows a direct four electron transfer mechanism, which is in contrast to that of the other two compositions. From the K-L plots, the linearity and parallelism are usually considered an indication of first-order reaction kinetics.[44] Based on the results, the 3:1 composition was good and was used for further electrochemical investigations towards the ORR. Interestingly, it was also reported that a 20-30 atomic wt. % of Rh might be a better composition for the ORR[43], which was well correlated with the present investigation.

ORR activity on Au-Rh (3:1)

Fig. 3 shows the CV data of the supportless and carbon supported Au-Rh (3:1) catalysts. Two distinct major regions were observed during the anodic sweep: (i) a broad double layer region between -0.6 and -0.2 V; (ii) an oxide layer (Au-O(H)) formation at the higher potential region (0.3 to 0.5 V). In the cathodic sweep an oxide reduction peak was clearly observed between 0.2 to -0.2 V.[42] A broad and defined reduction peak was observed for the supportless Au-Rh (3:1) with a peak current density of 7.5 mA/cm^2, which was comparatively higher than the reported literature values for Au-based catalysts.[14, 15, 23] For Au-Rh (3:1)/VC, a less intense reduction peak with a current density of ~2.5 mA/cm^2 showed poor ORR kinetics compared to Au-Rh (3:1) NCs. The calculated ECSA was found to be 32.7 m^2/g for Au-Rh (3:1) catalyst which is 1.5 times higher than Au-Rh(3:1)/VC (19.2 m^2/g) and was comparable to the reported values.[1] This observed higher ECSA might be due to the availability of more active catalyst sites in the supportless nanostructure.

Fig. 4a shows the polarization curves of the supportless and Vulcan carbon-supported Au-Rh (3:1) catalysts recorded at 2400 rpm. From the polarization curves, three distinct regions were observed: (i) the kinetic controlled region observed between 0.5 to -0.1 V with the reduction peak of Au-oxide; (ii) the mixed kinetic and diffusion controlled region, i.e., the sloppy region from -0.1 V to -0.18 V, where the reduction current is controlled by both mass transfer

and the kinetics of the electron transfer mechanism; and (iii) the mass transfer (diffusion) controlled region was observed below -0.18 V.[43] The limiting current densities were 4.41 and 3.88 mA/cm^2 for Au-Rh (3:1) and Au-Rh (3:1)/VC, respectively. The higher onset (-0.05 V) and half-wave potential ($E_{1/2}$, -0.11 V) values were obtained for Au-Rh (3:1) NCs that were comparatively 30 mV (Onset: -0.08 V) and 60 mV ($E_{1/2}$, -0.11 V) more positive than that of Au-Rh (3:1)/VC. **Fig. 4b** presents the K-L plots and shows parallel behavior with a slope of 10.86 and 13.11 for Au-Rh (3:1) NC and Au-Rh (3:1)/VC, respectively. From the K-L slopes, the '*n*' values were 4.1 for SL Au-Rh (3:1) NCs and 3.9 for Au-Rh (3:1)/VC, suggesting that both the catalysts follow a direct 4-electron transfer mechanism. **Figs. 5a & 5c** show linear scan voltammograms with increasing trend of limiting current densities with respect to the electrode rotation rate confirms the influence of hydrodynamic (diffusion layer thickness) effects for both supportless and VC supported Au-Rh catalysts on RDE-GC electrode. In addition to that, the K-L plots (**Figs. 5b & 5d**) drawn at different potentials (-0.2, -0.4, -0.6, and -0.8 V vs. SHE) clearly indicates the ORR mechanism follows direct four electron transfer mechanism and the calculated '*n*' values are in the range of 3.4 to 4.1 for supportless and 3.2 to 3.9 for VC supported Au-Rh catalyst. In order to evaluate the catalytic activity, the kinetic current density (j_k) was calculated using the following equation,[45]

$$j_k = \frac{j_d \times j_p}{j_d - j_p}$$

where j_p is the measured current density at -0.1 V vs. SHE and j_d is the disc current density at the limiting region. For Au-Rh (3:1) NC, the observed kinetic current density (j_k) was found to be 1.41 mA/cm^2 at -0.1 V, which is nearly 2 times higher than that of the Au-Rh (3;1)/VC catalyst (0.71 mA/cm^2) and comparatively higher than the reported SnO_2-Au hybrid catalysts in alkaline media.[21]

Using the calculated kinetic current density values (j_k), the mass transfer-corrected Tafel plots were constructed and the Tafel slopes were determined at low and higher overpotential regions and presented in **Fig. 6**. Tafel slope values at low overpotential region were found to be 57 and 69 mV/dec and at higher over potential region 119 and 114 mV/dec for supportless and carbon supported Au-Rh (3:1) catalysts, respectively. At low overpotential, the obtained Tafel slope values are close to -60 mV dec^{-1}, which indicates that the ORR mechanism follows one electron transfer is the rate determining step and at higher overpotential the values are around -120 mV dec^{-1} reveals that the two electron transfer is the rate determining step.[46, 47] From the reported literature, two Tafel slope regions of, (i) 60 mV dec^{-1} corresponding to O_2 electro-reduction at the oxidized (Pt-OH) surface (ii) 120 mV dec^{-1} observed for clean Pt surface in an acidic environment. Hence, it is clearly suggesting that the surface properties of Au-Rh catalysts are quite similar to that of clean Pt and indicating the first electron transfer as the rate limiting step in reduction of oxygen.[48] **Fig. 7a** shows the number of electrons transferred (n) per oxygen molecule during reduction process at different potential values. A higher exchange current density (i_0) was obtained for Au-Rh (3:1) NCs (2.19×10^{-5} A/cm^2) than Au-Rh (3:1)/VC (1.0×10^{-5} A/cm^2). **Table 1** lists the calculated ORR kinetic parameters, such as limiting current density (j_d), onset potential, half wave potential, kinetic current density (j_k), Tafel slope (b), number of electrons transferred (n), mass, and specific activity values. It can be observed that kinetic current density, exchange current density and mass activity values are nearly twice for Au-Rh (3:1) compared to Au-Rh/VC. The lower Tafel slope value indicates a facile ORR kinetics for Au-Rh (3:1) and this in turn results in the direct 4-electron transfer mechanism. **Fig. 7b** shows the comparison of the mass activity (MA) of both the supportless and VC supported Au-Rh (3:1) catalysts with various reported alkaline ORR electrocatalysts from the literature.[17, 32, 38] Using these MA values, the intrinsic activity or specific activity (SA) values were calculated and found

to be 3.25 for Au-Rh (3:1) NCs and 3.0 A/m^2_{Au} for Au-Rh (3:1)/VC, which were comparatively higher than the reported Pt/C (MA: 58 mA/mg; SA: 0.1 mA/cm^2)[45] and other alkaline ORR electrocatalysts in KOH medium.[20, 39]

Durability of Au-Rh nanostructures

The durability of the electrocatalyst was evaluated by performing accelerated durability tests (ADT) i.e. by subjecting the working electrode to a specified number of continuous potential sweeps between -0.6 and 0.2 V at 0.1 V/s in N_2-saturated 0.5 M KOH at 25 °C. **Figs. 8a and 8b** show the ADT-CVs for both the supportless and carbon supported Au-Rh catalysts under similar conditions. During the ADT, the Au-oxide reduction peak became broader for Au-Rh (3:1) NC (**Fig. 8a**) and sharper for the carbon supported Au-Rh (3:1) catalysts (**Fig. 8b**). After 10000 potential cycles, the calculated ECSA increased by ~20-30 % for both catalysts, which might be due to structural reformation (active site regeneration). **Figs. 8c & 8d** clearly show the durability of the electrocatalysts in terms of the percentage of ECSA retained after ADT. In fact, the ECSA of the supportless catalyst was almost 15 % higher than the carbon supported catalyst after 10000 potential cycles. When the ADT was extended to the other Au-Rh compositions 1:1 and 1:3, we observed approximately 20 to 50 % decrease in ECSA after 5000 potential cycles (graphs are not shown). The ADT-LSVs were recorded in the O_2 saturated 0.5 M KOH solution at a scan rate of 0.01 V/s at 2400 rpm. **Fig. 8e** shows the LSV profiles before and after 10000 potential cycles for Au-Rh (3:1) NC which retains ~89 % of its initial limiting current density at 10000^{th} cycle while Au-Rh (3:1)/VC (**Fig. 8f**) retains only ~83 % after 10000 potential cycles. On the other hand, looking into the half-wave potential values, an 80 mV negative shift was observed for the Au-Rh (3:1) NC, which was almost 1.5 times (180 mV) better than Au-Rh (3:1)/VC. The TEM image (Fig. 9a) shows that there is no appreciable change in particle size of

supportless Au-Rh catalyst after ADT and clearly depicted from the corresponding histogram (Fig. 9c). But, the Au-Rh/VC has increased in particles size nearly 2 nm after 10000 cycles which is resulted in decreased LSV-ORR current compared to the supportless catalyst. In addition to that the Au-Rh/VC, has increased in surface area upon continuous potential cycling thus might be expected due to the chemisorbed CO[49] (Journal of The Electrochemical Society, 160 (4) F381-F388 (2013)) (which eventually reduces the available and free active sites). As a result the ORR activity decreases upon cycling for supported catalysts. To summarize the supportless Au-Rh (3:1) showed a remarkable stability compared to the carbon supported catalyst and also the retained activity after ADT was comparatively higher than that reported values for other alkaline ORR electrocatalysts, such as Au@Pd/RGO (~6 % ORR current loss after 1000 potential cycles)[50], Pt/C (~ 42 % ORR current loss after 1,500 potential cycles)[51], and NCo-GS-0.5 (40% loss in activity after 12000 potential cycles).[52]

Conclusion

Novel supportless and vulcan carbon supported Au-Rh bimetallic nanostructures were synthesized by a green chemical reduction approach without stabilizing agents which showed an enhanced electrocatalytic performance for the ORR in alkaline medium. From physiochemical characterizations, the mean crystallite size and elemental composition were determined. TEM clearly revealed the nanostructure morphology of Au-Rh and the uniform distribution of Au-Rh nanoparticles on carbon for the Au-Rh/VC catalyst. From cyclic voltammetry studies, the ECSA was found to be 32.7 m^2/g and the limiting current density was observed to be 4.41 mA/cm^2 for Au-Rh (3:1) NC which were comparatively higher than the other supportless and carbon supported catalysts. The higher MA (106 mA/mg) and SA (3.25 A/m^2_{Au}) were obtained for the Au-Rh NC and the ORR kinetic parameters were calculated and presented. The durability studies

clearly showed that both the supportless and VC supported Au-Rh (3:1) electrocatalysts possess an improved life-time in terms of ECSA and the ORR limiting current density, even after 10000 potential cycles. Therefore, this study proves that the Au-Rh (3:1) nanostructures have great potential to catalyze the ORR with enhanced activity and stability for alkaline fuel cells.

Acknowledgements

This study was supported by the '*National Research Foundation*' (NRF) funded by the Ministry of Education, Science and Technology (MEST), Government of the Republic of Korea (Grant No. 2014R1A2A1A01001974). S.B. wishes to thank The Korean Federation of Science and Technology Societies (KOFST, Republic of Korea) for the post of 'Invited Scientist' through the '*Brain Pool Program*', and Sri Chandrasekharendra Saraswathi Viswa Mahavidyalaya (Deemed University), Enathur, Kanchipuram, India for the sanction of 'Sabbatical Leave' during 2014-2015. B.N. wishes to thank HySA Systems, SAIMAC for the award of 'postdoctoral research fellowship' and for providing the HRTEM facility.

References

1. Guo, S.; Zhang, S.; Sun, S. Tuning nanoparticle catalysis for the oxygen reduction reaction, *Angew. Chem. Int. Ed* **2013**, *52*, 8526-8544.
2. Markovic, N.M.; Schmidt, T.J.; Stamenkovic, V.; Ross, P.N. Oxygen reduction reaction on Pt and Pt bimetallic surfaces: A Selective review, *Fuel Cells* **2001**, *1*, 105-116.
3. Katsounaros, I.; Cherevko, S.; Zeradjanin, A.R.; Mayrhofer, K.J.J. Oxygen electrochemistry as a cornerstone for sustainable energy conversion, *Angew. Chem. Int. Ed* 2014, *53*, 102-121.

4. Noto, V.D.; Negro, E.; Keti Vezzu, K.; Bertasi, F.; Nawn, G. Origins, Developments and perspectives of carbon nitride-based electrocatalysts for application in low-temperature FCs, *Electrochem. Soc. Interf. Summ*. 2015, *2015*, 59-64.
5. Noto, V.D.; Negro, E.; Polizzi, S.; Vezzu, K,; Toniolo, L.; Cavinato, G. Synthesis, studies and fuel cell performance of "core-shell" electrocatalysts for oxygen reduction reaction based on a $PtNi_x$ carbon nitride "shell" and a pyrolyzed polyketone nanoball "core", *Int. J. Hydrogen Energy*, **2014**, *39*, 2828-2841.
6. Negro, E.; Polizzi, S.; Vezzu, K,; Toniolo, L.; Cavinato, G.; Noto, V.D. Interplay between morphology and electrochemical performance of "core-shell" electrocatalysts for oxygen reduction reaction based on a $PtNi_x$ carbon nitride "shell" and a pyrolyzed polyketone nanoball "core", *Int. J. Hydrogen Energy*, 2014, *39*, 2812-2827.
7. Morozan, A.; Jousselme, B.; Palacin, S. Low-platinum and platinum-free catalysts for the oxygen reduction reaction at fuel cell cathodes, *Energy Environ. Sci*. **2011**, *4*, 1238-1254.
8. Wang, B. Recent development of non-platinum catalysts for oxygen reduction reaction, *J. Power Sources* **2005**, *152*, 1-15.
9. Quaino, P.; Luque, N.B.; Nazmutdinov, R.; Santos, E.; Schmickler, W. Why is gold such a good catalyst for oxygen reduction in alkaline media? *Angew. Chem. Int. Ed*. **2012**, *51*, 12997-13000.
10. Raj, C.R.; Abdelrahman, A.I.; Ohsaka, T. Gold nanoparticle-assisted electroreduction of oxygen, *Electrochem. Commun*. **2005**, *7*, 888-893.
11. Shim, J.H.; Kim, J.; Lee, C.; Lee, Y. Electrocatalytic activity of gold and gold Nanoparticles improved by electrochemical pretreatment, *J. Phys. Chem. C* **2011**, *115*, 305-309.

12. Zhang, G.R.; Zhao, D.; Feng, Y.Y.; Zhang, B.; Su, D.S.; Liu, G.; Xu, B.Q. Catalytic Pt-on-Au nanostructures: Why Pt becomes more active on smaller Au particles, *ACS Nano*, **2012**, *6*, 2226-2236.

13. Kuai, L.; Geng, B.; Wang, S.; Zhao, Y.; Luo, Y.; Jiang, H. Silver and Gold Icosahedra: One-Pot Water-Based synthesis and their superior Performance in the electrocatalysis for oxygen reduction reactions in alkaline media, *Chem. Eur. J*. **2011**, *17*, 3482-3489.

14. Manivannan, S.; Ramaraj, R. Electrodeposited nanostructured raspberry-like gold-modified electrodes for electrocatalytic applications, J. Nanopart. Res. **2013**, *15*, 1-13.

15. Yin, H.; Tang, H.; Wang, D.; Gao, Y.; Tang, Z. Facile Synthesis of surfactant-free Au cluster/graphene hybrids for high-performance oxygen reduction reaction, *ACS Nano*, 2012, *6*, 8288-8297.

16. Narayanamoorthy, B.; Linkov, V.; Sita, C.; Pasupathi, S. Pt_3M (M: Co, Ni and Fe) bimetallic alloy nanoclusters as support-free electrocatalysts with improved activity and durability for dioxygen reduction in PEM fuel cells, *Electrocatal*. 2016, *7*, 400-410.

17. Praserthdam, S.; Balbuena, P.B. Effects of oxygen coverage, catalyst size, and core composition on Pt-alloy core-shell nanoparticles for the oxygen reduction reaction, *Catal. Sci. Technol.*, 2016, DOI: 10.1039/C5CY02287H.

18. Jalili, S.; Isfahani, A.Z.; R. Habibpour, DFT investigations on the interaction of oxygen reduction reaction intermediates with Au (100) and bimetallic Au/M (100) (M = Pt, Cu, and Fe) surfaces, *Inter. J. Indust. Chem*. **2013**, *4*, 1-12.

19. Maye, M.M.; Kariuki, N.N.; Luo, J.; Han, L.; Njoki, P.; Wang, L.; Lin, Y.; Naslund, H.R.; Zhong, C.J. Electrocatalytic reduction of oxygen: Gold and gold-platinum nanoparticle catalysts prepared by two-phase protocol, *Gold Bull*. **2004**, *37*, 217-223.

20. Song, Y.; Liu, K.; Chen, S. AgAu bimetallic Janus nanoparticles and their electrocatalytic activity for oxygen reduction in alkaline media, *Langmuir*, **2012**, *28*, 17143-17152.

21. Chen, W.; Ny, D.; Chen, S. SnO_2-Au hybrid nanoparticles as effective catalysts for oxygen electroreduction in alkaline media, *J. Power Sources*, **2010**, *195*, 412-418.

22. El-Deab, M.S.; Ohsaka, T. Electrocatalysis by design: Effect of the loading level of Au nanoparticles–MnOx nanoparticles binary catalysts on the electrochemical reduction of molecular oxygen, *Electrochim. Acta*, **2007**, *52*, 2166-2174.

23. Kuai, L.; Yu, X.; Wang, S.; Sang, Y.; Geng, B. Au–Pd Alloy and Core–Shell Nanostructures: One-Pot Coreduction Preparation, Formation Mechanism, and Electrochemical Properties, *Langmuir*, **2012**, *28*, 7168-7173.

24. Hong, J.W.; Lee, Y.W.; Kim, M.; Kang, S.W.; Han, S.W. One-pot synthesis and electrocatalytic activity of octapodal Au-Pd nanoparticles, *Chem. Commun*. **2011**, *47*, 2553-2555.

25. Jena, B.K.; Raj, C.R. Synthesis of Flower-like Gold Nanoparticles and Their Electrocatalytic Activity Towards the Oxidation of Methanol and the Reduction of Oxygen, *Langmuir*, **2007**, *23*, 4064-4070.

26. Levy, O.; Chepulskii, R.V.; Hart, G.L.W.; Curtarolo, S. The new face of rhodium alloys: revealing ordered structures from first principles, *J. Am. Chem. Soc*. **2010**, *132*, 833-837.

27. Qi, Y.; Wu, J.; Zhang, H.; Jiang, Y.; Jin, C.; Fu, M.; Yang, H.; Yang, D. Facile synthesis of Rh-Pd alloy nanodendrites as highly active and durable electrocatalysts for oxygen reduction reaction, *Nanoscale*, **2014**, *6*, 7012-7018.

28. Yan, Y.; Zhan, F.; Du, J.; Jiang, Y.; Jin, C.; Fu, M.; Zhang, H.; Yang, D. Kinetically-controlled growth of cubic and octahedral Rh-Pd alloy oxygen reduction electrocatalysts with high activity and durability, *Nanoscale*, **2015**, *7*, 301-307.

29. Narayanamoorthy, B.; Datta, K.K.R.; Eswaramoorthy, M.; Balaji, S. Highly active and stable Pt_3Rh nanoclusters as supportless electrocatalyst for methanol oxidation in direct methanol fuel cells, *ACS Catal*. **2014**, *4*, 3621-3629.

30. Lima, F.H.B.; Profeti, D.; Chatenet, M.; Riello, D.; Ticianelli, E.A.; Gonzalez, E.R. Electro-oxidation of ethanol on Rh/Pt and Ru/Rh/Pt sub-monolayers deposited on Au/C nanoparticles, *Electrocatal*. 2010, *1*, 72-82.

31. Yuan, Q.; Zhou, Z.; Zhuang, J.; Wang, X. Seed Displacement, Epitaxial synthesis of Rh/Pt bimetallic ultrathin nanowires for highly selective oxidizing ethanol to CO_2, *Chem. Mater*. **2010**, *22*, 2395-2402.

32. Parka, K.W.; Han, D.S.; Sung, Y.E. PtRh alloy nanoparticle electrocatalysts for oxygen reduction for use in direct methanol fuel cells, *J. Power Sources*, **2006**, *163*, 82-86.

33. Noto, V.D.; Negro, E. A new Pt–Rh carbon nitride electrocatalyst for the oxygen reduction reaction in polymer electrolyte membrane fuel cells: Synthesis, characterization and single-cell performance, *J. Power Sources*, **2010**, *195*, 638-648.

34. Friebel, D.; Miller, D.J.; Nordlund, D.; Ogasawara, H.; Nilsson, A. Degradation of bimetallic model electrocatalysts: An *In-Situ* X-Ray absorption spectroscopy study, *Angew. Chem. Int. Ed*. **2011**, *50*, 10190-10192.

35. Narayanamoorthy, B.; Datta, K.K.R.; Eswaramoorthy, M.; Balaji, S. Self-stabilized Pt-Rh bimetallic nanoclusters as durable electrocatalysts for dioxygen reduction in PEM fuel cells, *RSC Adv*. **2014**, *4*, 55571-55579.

36. Xu, C.; Tian, Z.; Chen, Z.; Jiang, S.P. Pd/C promoted by Au for 2-propanol electrooxidation in alkaline media, *Electrochem. Commun*. **2008**, *10*, 246-249.

37. M. Tsuji, Y. Nakashima, A. Yajima, M. Hattori, *CrystEngComm*, **2015**, *17*, 6955-6961.

38. Li, Y.; Song, Y.Y.; Yang, C.; Xia, X.H. Hydrogen bubble dynamic template synthesis of porous gold for nonenzymatic electrochemical detection of glucose, *Electrochem. Commun*. **2007**, *9*, 981-988.

39. Gui-Rong, Z.; Bo-Qing, X. Nanosize effect of Au catalyst for electrochemical reduction of oxygen in alkaline electrolyte, *Chin. J. Catal*. **2013**, *344*, 942-948.

40. Narayanamoorthy, B.; Datta, K.K.R.; Balaji, S. Kinetics and mechanism of electrochemical oxygen reduction using Platinum/clay/Nafion catalyst layer for polymer electrolyte membrane fuel cells, *J. Colloid Interf. Sci*. **2012**, *387*, 213-220.

41. Lee, C.L.; Chiou, H.P.; Syu, C.M.; Wu, C.C. Silver triangular nanoplates as electrocatalyst for oxygen reduction reaction, *Electrochem. Commun*. **2010**, *12*, 1609-1613.

42. Oliveira, R.T.S.; Santos, M.C.; Nascent, P.A.P.; Bulhoes, L.O.S.; Pereira, E.C. Nanogravimetric and Voltammetric Studies of a Pt-Rh alloy Surface and its Behavior for Methanol Oxidation, *Int. J. Electrochem. Sci*. **2008**, *3*, 970-979.

43. Hebie, S.; Kokoh, K.B.; Servat, K.; Napporn, T.W. Shape-dependent electrocatalytic activity of free gold nanoparticles toward glucose oxidation, *Gold Bull*. **2013**, *46*, 311-318.

44. Li, W.; Haldar, P. Highly active carbon supported core-shell PtNi@Pt nanoparticles for oxygen reduction reaction, *Electrochem. Solid-State Lett*. **2010**, *13*, B47-B49.

45. Zhang, Z.; More, K.L.; Sun, K.; Wu, Z.; Li, W. Preparation and characterization of PdFe nanoleaves as electrocatalysts for oxygen reduction reaction, *Chem. Mater*. **2011**, *23*, 1570-1577.

46. Narayanamoorthy, B.; Panneerselvam, N.; Sita, C.; Pasupathi, S.; Balaji, S.; Moon, I.S. Enhanced stabilities of Ag electrocatalyst as self-standing and multiwalled carbon nanotube supported nanostructures for oxygen reduction in alkaline medium, *J. Electrochem. Soc*. **2016**, *163*, H313-H320.

47. Shypunov, I.; Kongi, N.; Kozlova, J.; Matisen, L.; Ritslaid, P.; Sammelselg, V.; Tammeveski, K. Enhanced oxygen reduction reaction activity with electrodeposited Ag on manganese oxide-graphene supported electrocatalyst, *Electrocatal*. **2015**, *6*, 465-471.

48. Narayanamoorthy, B.; Pavan Kumar, B.V.V.S.; Eswaramoorthy, M.; Balaji, S. Oxygen reduction reaction catalyzed by platinum nanonetwork prepared by template free one step synthesis for polymer electrolyte membrane fuel cells, Mater. Res. Bull. **2014**, *55*, 137-145.

49. Wang, Y.; Wilkinson, D.P.; Zhang, J. Noncarbon support materials for polymer electrolyte membrane fuel cell electrocatalysts, *Chem. Rev*., **2011**, *111*, 7625-7651.

50. Li, S.S.; Wang, A.J.; Hu, Y.Y.; Fang, K.M.; Chen, J.R.; Feng, J.J. One-step, seedless wet-chemical synthesis of gold@palladium nanoflowers supported on reduced graphene oxide with enhanced electrocatalytic properties, *J. Mater. Chem*. A, **2014**, *2,* 18177-18183.

51. Tang, Q.; Jiang, L.; Qi, J.; Jiang, Q.; Wang, S.; Sun, G. One step synthesis of carbon-supported Ag/Mn_yO_x composites for oxygen reduction reaction in alkaline media, *Appl. Catal. B* **2011**, *104*, 337-345.

52. Jin, J.; Fu, X.; Liu, Q.; Zhang, J. A highly active and stable electrocatalyst for the oxygen reduction reaction based on a graphene-supported g-C_3N_4@cobalt oxide core-shell hybrid in alkaline solution, *J. Mater. Chem. A*, **2013**, *1*, 10538-10545.

Figure Captions

Fig. 1 XRD patterns of the supportless and VC supported Au-Rh (3:1) catalysts.

Fig. 2 TEM images of the supportless (a & c) and Vulcan carbon supported (b & d) Au-Rh (3:1) catalysts with corresponding histograms (e & f). Inset: HR-TEM of supportless Au-Rh (Fig. 2a) and Au-Rh/VC (Fig. 2b).

Fig. 3 Cyclic voltammograms of the supportless and VC supported Au-Rh (3:1) in N_2 saturated 0.5 M KOH at a scan rate of 0.1 V/s at 25 °C.

Fig. 4 (a) RDE-Linear scan voltammograms of the supportless Au-Rh (3:1) and Au-Rh (3:1)/VC in O_2 saturated 0.5 M KOH at a scan rate of 0.01 V/s at 25 °C in 2400 rpm and (b) corresponding K-L plots.

Figs. 5 RDE-Linear scan voltammograms at different rotation rates and K-L plots at different potentials for supportless Au-Rh (3:1) (a & b) and Au-Rh (3:1)/VC (c & d) in O_2 saturated 0.5 M KOH at a scan rate of 0.01 V/s at 25 °C.

Fig. 6 Mass transfer corrected Tafel plots of the supportless Au-Rh (3:1) and Au-Rh (3:1)/VC in O_2 saturated 0.5 M KOH at a scan rate of 0.01 V/s at 25 °C in 2400 rpm.

Fig. 7 (a) Number of electrons transferred versus applied potential for both supportless Au-Rh (3:1) and Au-Rh (3:1)/VC in O_2 saturated 0.5 M KOH at a scan rate of 0.01 V/s; (b) Comparison of the mass activity of Au-Rh catalysts with different alkaline ORR electrocatalysts from various reported literatures.

Fig. 8 Cyclic voltammograms of (a) supportless Au-Rh (3:1) NCs; (b) Au-Rh (3:1)/VC in N_2 saturated 0.5 M KOH at 25 °C after ADT potential cycling; Linear scan voltammograms of (c) supportless Au-Rh (3:1) NCs; (d) Au-Rh (3:1)/VC in O_2 saturated 0.5 M KOH at 25 °C after ADT potential cycling; (e) comparison of the percentage of normalized ECSA after ADT and (f) comparison of percentage of normalized ORR limiting current after ADT potential cycling.

Fig. 9 TEM images of (a) supportless Au-Rh and (b) Au-Rh/VC catalysts after accelerated durability tests with corresponding histograms (c) and (d) respectively.

535

536 **Fig. 1**

537

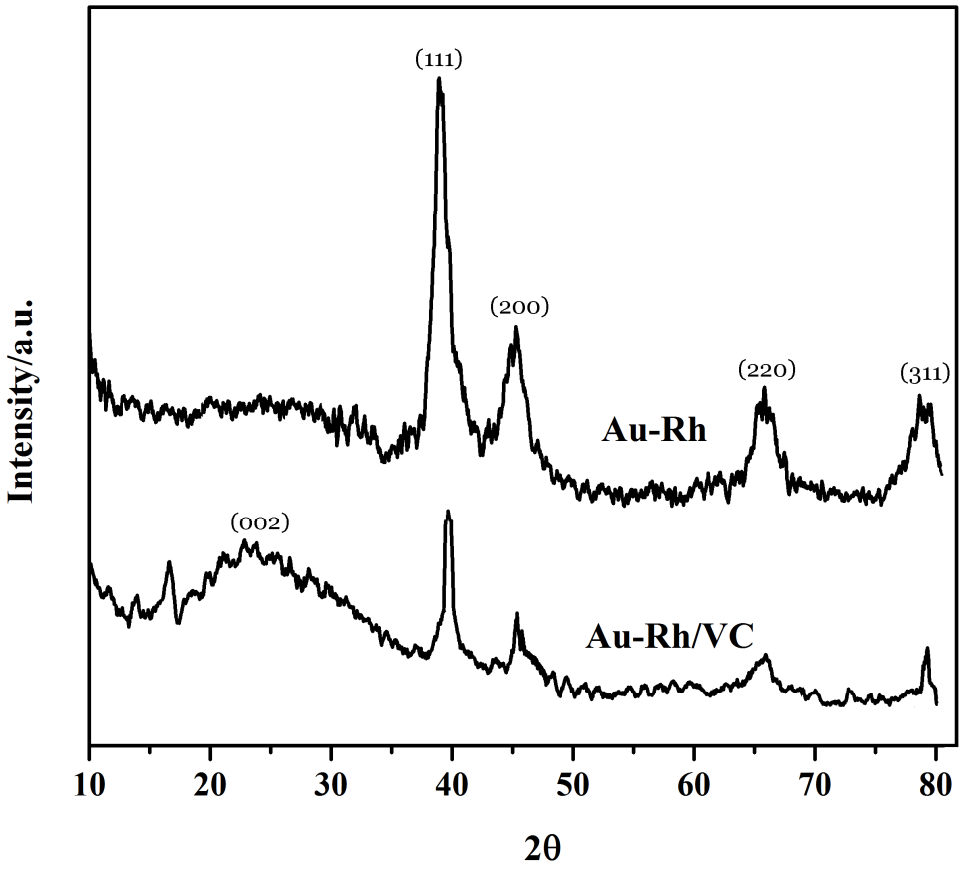

Fig. 2

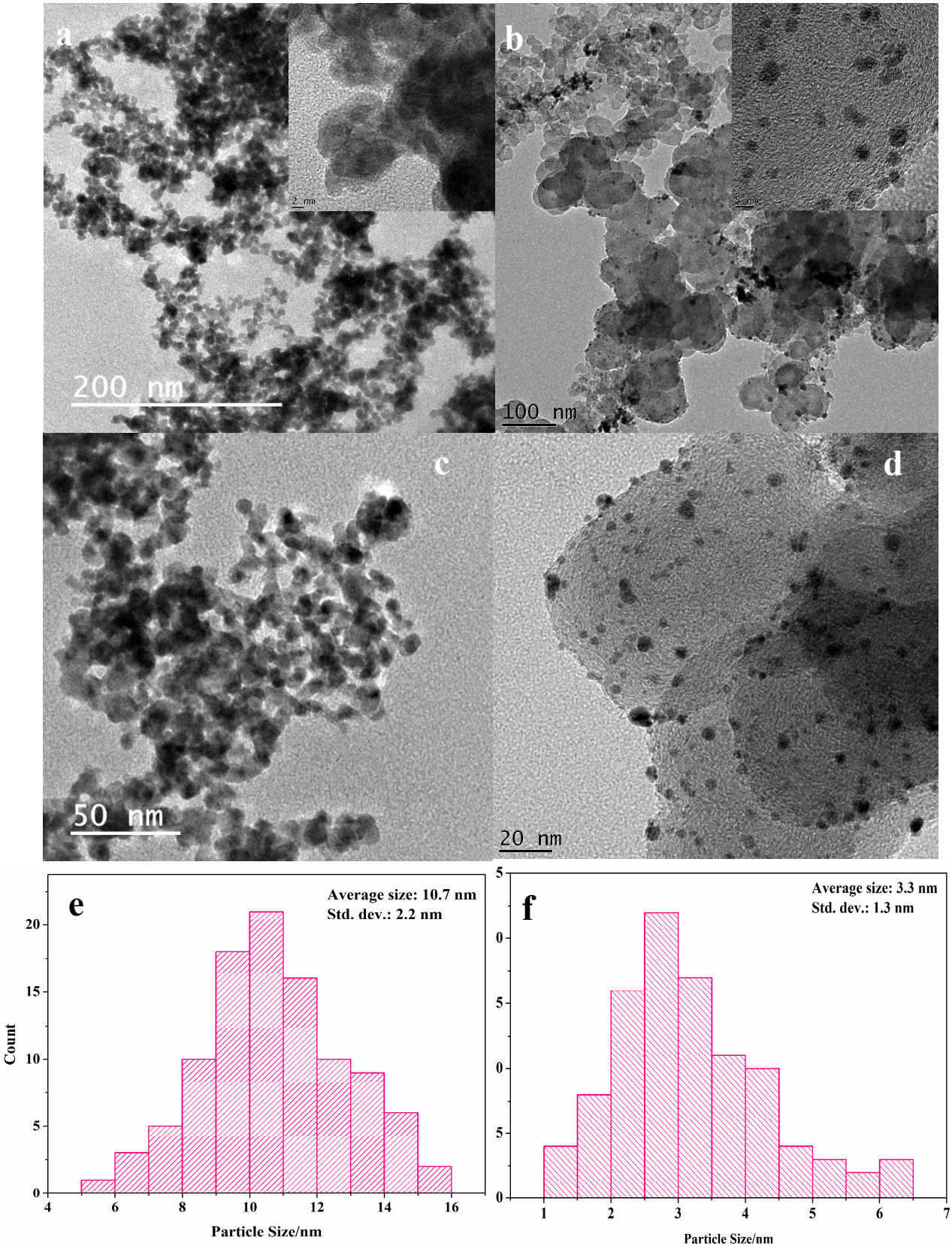
a
200 nm
b
100 nm
c
50 nm
d
20 nm
e
Average size: 10.7 nm
Std. dev.: 2.2 nm
Count
Particle Size/nm
f
Average size: 3.3 nm
Std. dev.: 1.3 nm
Particle Size/nm

Fig. 3

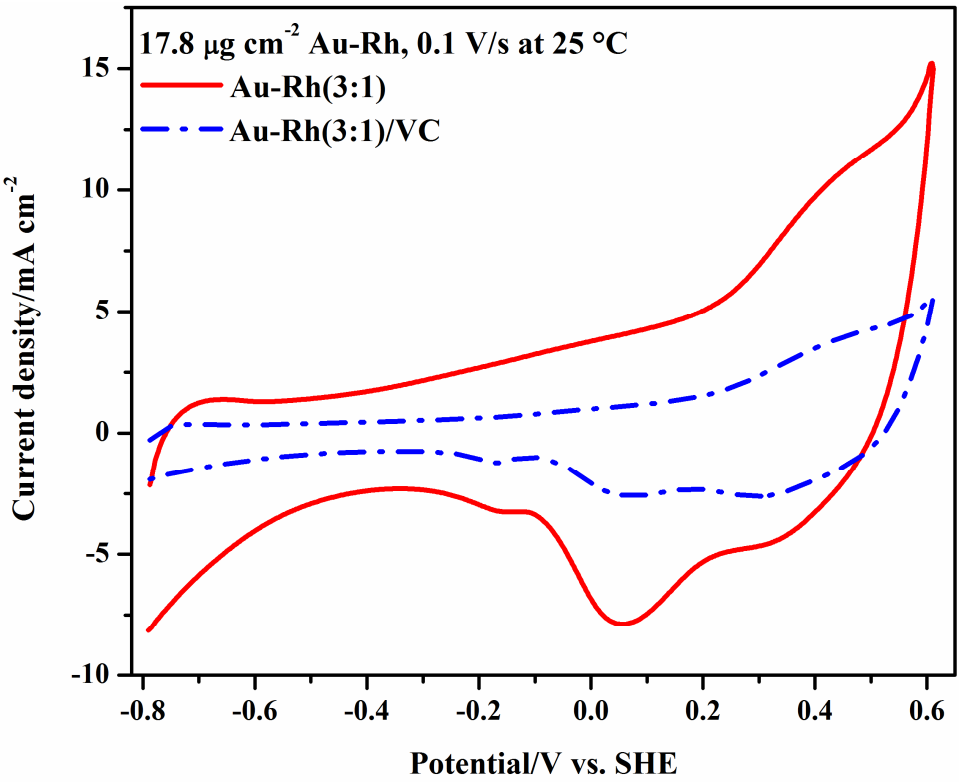
17.8 μg cm-2 Au-Rh, 0.1 V/s at 25 °C
Au-Rh(3:1)
Au-Rh(3:1)/VC
Current density/mA cm-2
Potential/V vs. SHE
15
10
5
0
-5
-10
-0.8
-0.6
-0.4
-0.2
0.0
0.2
0.4
0.6

Fig. 4

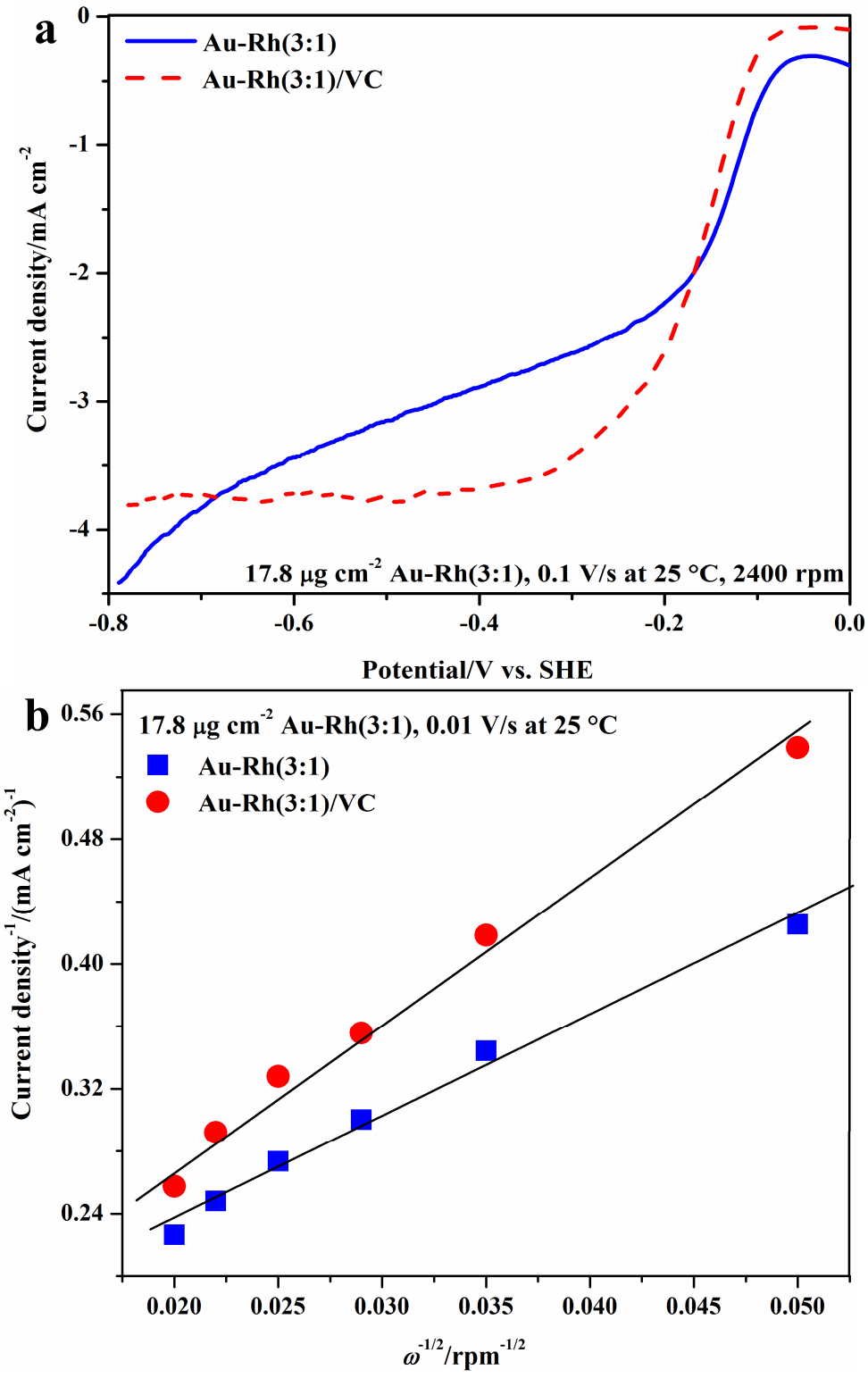
a
Au-Rh(3:1)
Au-Rh(3:1)/VC
Current density/mA cm-2
17.8 μg cm-2 Au-Rh(3:1), 0.1 V/s at 25 °C, 2400 rpm
Potential/V vs. SHE
b
17.8 μg cm-2 Au-Rh(3:1), 0.01 V/s at 25 °C
Au-Rh(3:1)
Au-Rh(3:1)/VC
Current density-1/(mA cm-2)-1
ω-1/2/rpm-1/2

Fig. 5

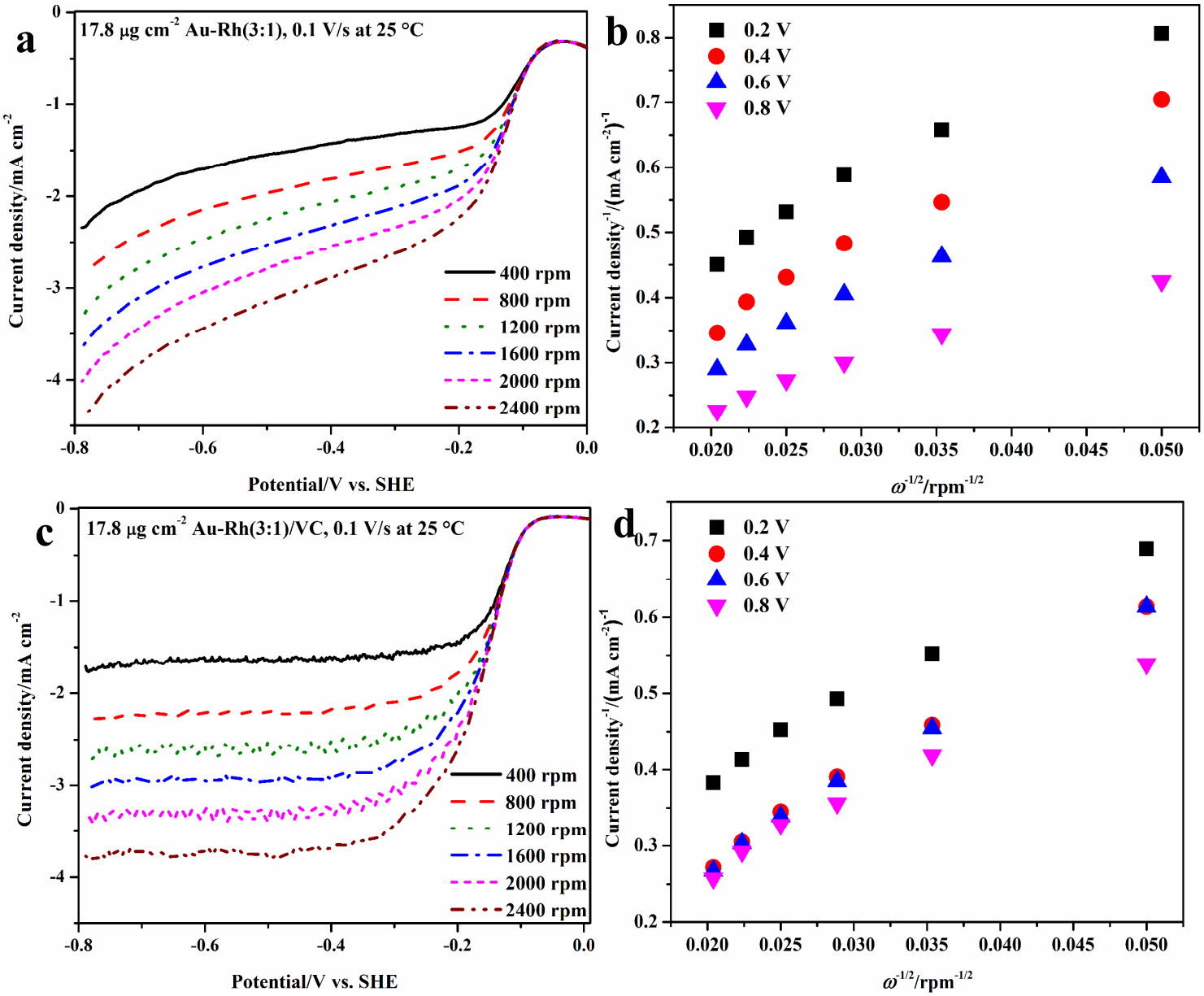
a
17.8 μg cm-2 Au-Rh(3:1), 0.1 V/s at 25 °C
Current density/mA cm-2
Potential/V vs. SHE
400 rpm
800 rpm
1200 rpm
1600 rpm
2000 rpm
2400 rpm
b
0.2 V
0.4 V
0.6 V
0.8 V
Current density-1/(mA cm-2)-1
ω-1/2/rpm-1/2
c
17.8 μg cm-2 Au-Rh(3:1)/VC, 0.1 V/s at 25 °C
Current density/mA cm-2
Potential/V vs. SHE
400 rpm
800 rpm
1200 rpm
1600 rpm
2000 rpm
2400 rpm
d
0.2 V
0.4 V
0.6 V
0.8 V
Current density-1/(mA cm-2)-1
ω-1/2/rpm-1/2

Fig. 6

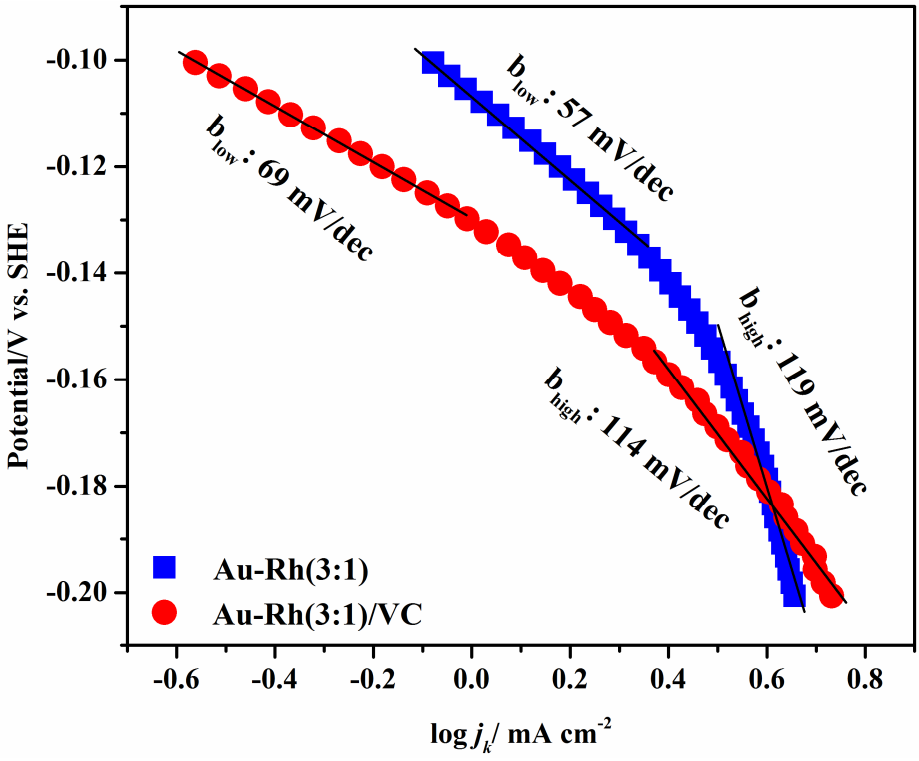
Potential/V vs. SHE
-0.10
-0.12
-0.14
-0.16
-0.18
-0.20
-0.6
-0.4
-0.2
0.0
0.2
0.4
0.6
0.8
log j_k/ mA cm^{-2}
b_{low} : 57 mV/dec
b_{high} : 119 mV/dec
b_{low} : 69 mV/dec
b_{high} : 114 mV/dec
Au-Rh(3:1)
Au-Rh(3:1)/VC

Fig. 7

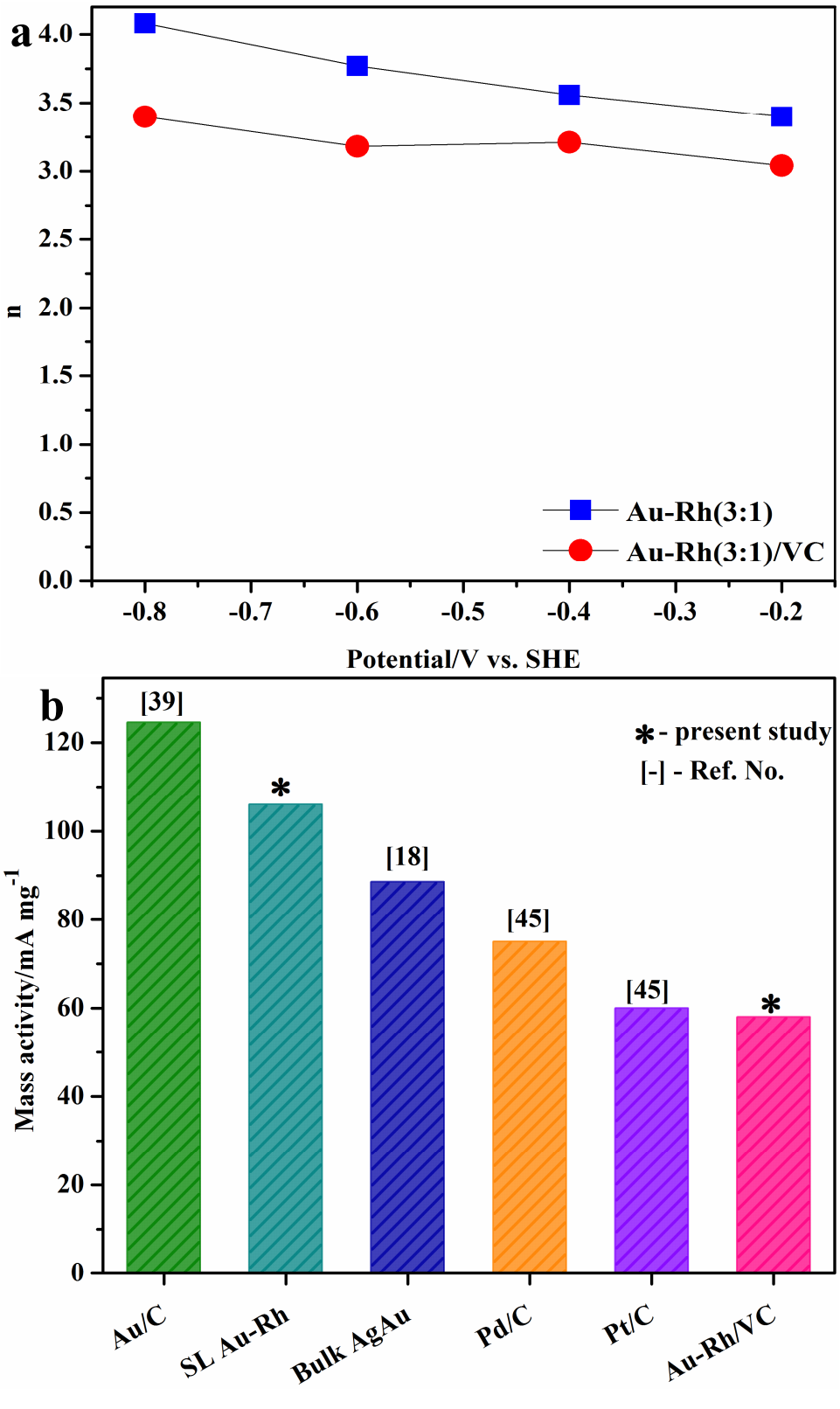
a
n
Potential/V vs. SHE
Au-Rh(3:1)
Au-Rh(3:1)/VC
b
Mass activity/mA mg-1
∗- present study
[-] - Ref. No.
[39]
[18]
[45]
[45]
Au/C
SL Au-Rh
Bulk AgAu
Pd/C
Pt/C
Au-Rh/VC

Fig. 8

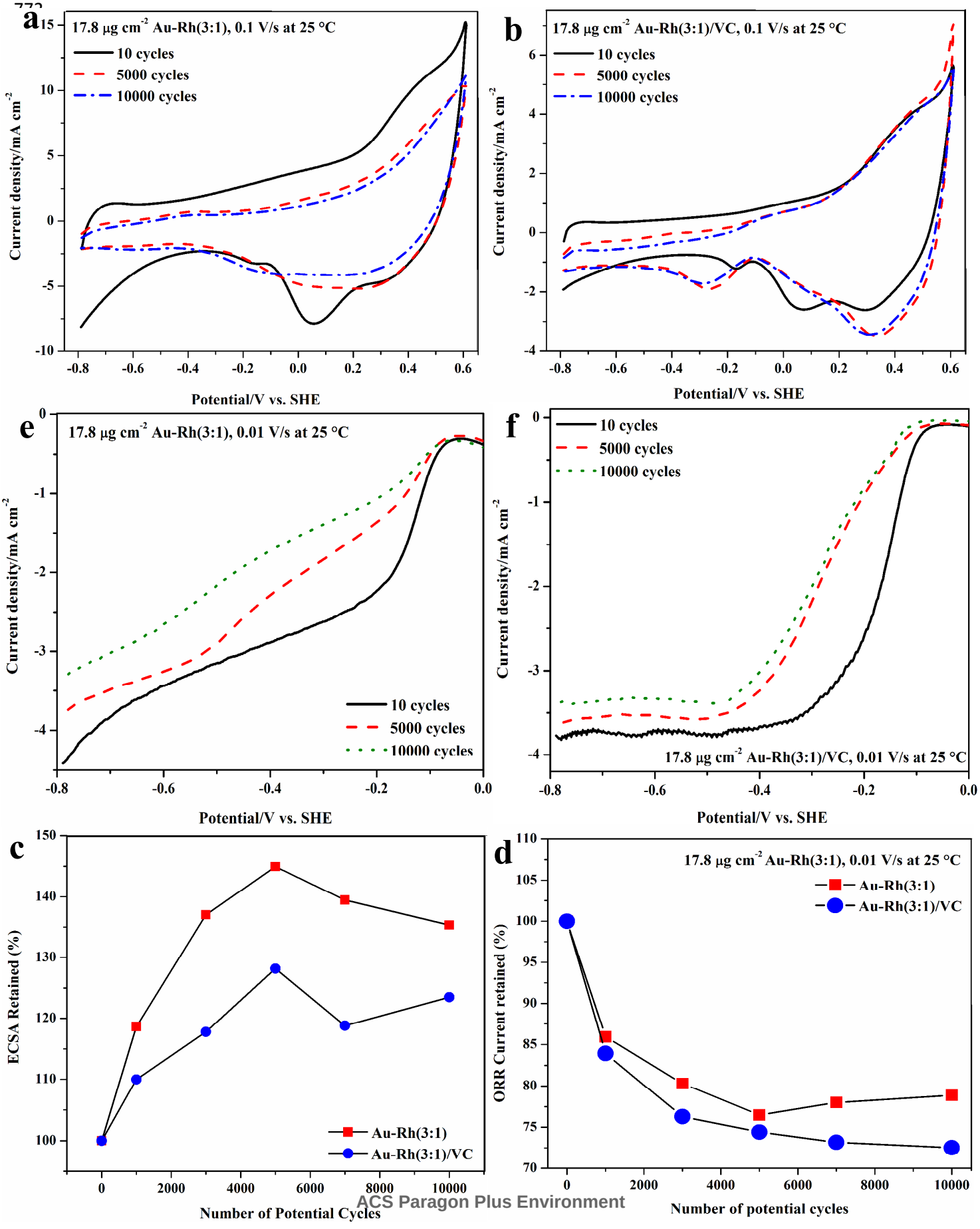
a
17.8 μg cm-2 Au-Rh(3:1), 0.1 V/s at 25 °C
10 cycles
5000 cycles
10000 cycles
Current density/mA cm-2
Potential/V vs. SHE
b
17.8 μg cm-2 Au-Rh(3:1)/VC, 0.1 V/s at 25 °C
10 cycles
5000 cycles
10000 cycles
Current density/mA cm-2
Potential/V vs. SHE
e
17.8 μg cm-2 Au-Rh(3:1), 0.01 V/s at 25 °C
10 cycles
5000 cycles
10000 cycles
Current density/mA cm-2
Potential/V vs. SHE
f
10 cycles
5000 cycles
10000 cycles
17.8 μg cm-2 Au-Rh(3:1)/VC, 0.01 V/s at 25 °C
Current density/mA cm-2
Potential/V vs. SHE
c
Au-Rh(3:1)
Au-Rh(3:1)/VC
ECSA Retained (%)
Number of Potential Cycles
d
17.8 μg cm-2 Au-Rh(3:1), 0.01 V/s at 25 °C
Au-Rh(3:1)
Au-Rh(3:1)/VC
ORR Current retained (%)
Number of potential cycles

Fig. 9

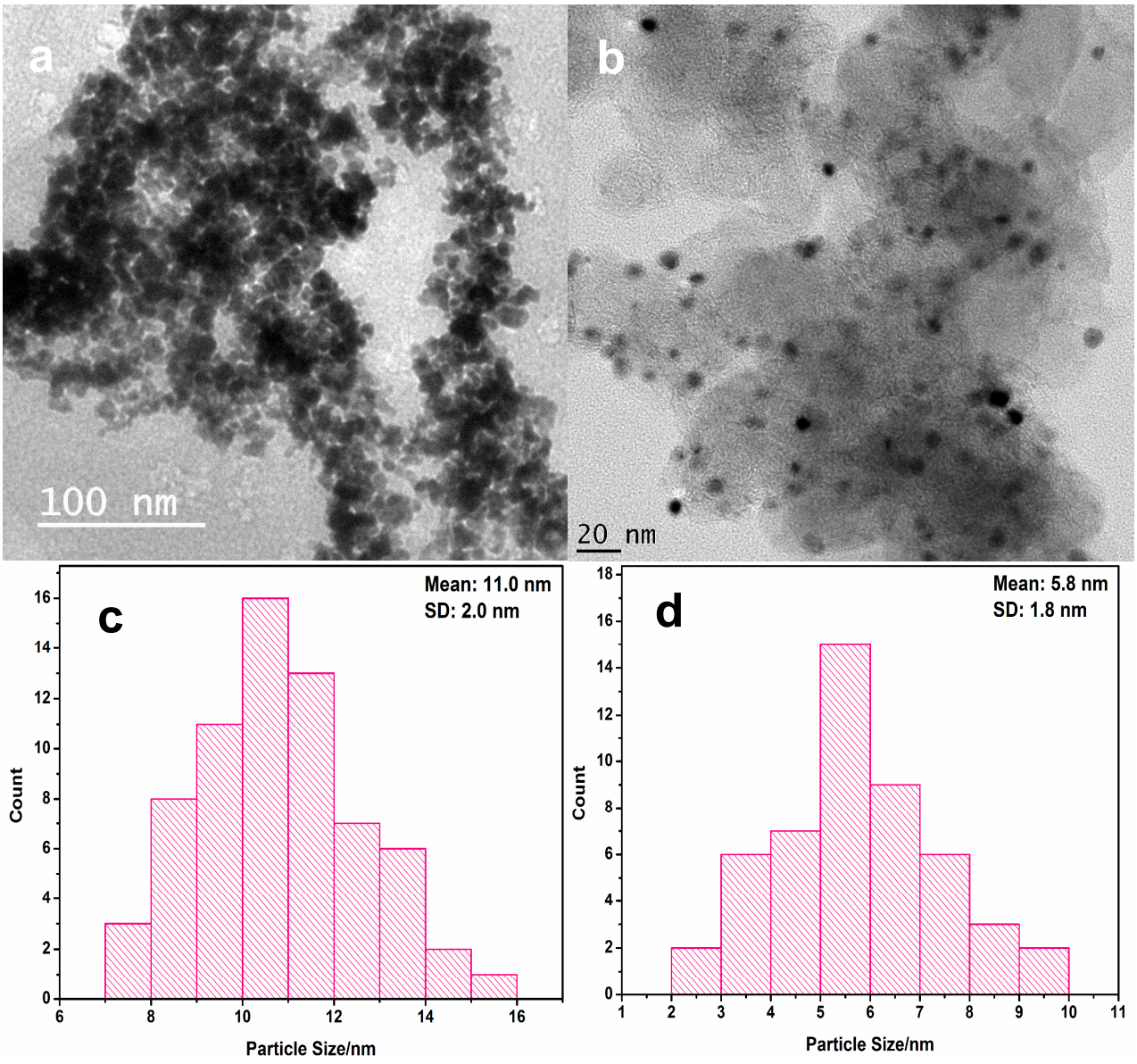
a
100 nm
b
20 nm
c
Mean: 11.0 nm
SD: 2.0 nm
Count
Particle Size/nm
d
Mean: 5.8 nm
SD: 1.8 nm
Count
Particle Size/nm

Table 1 Summary of ORR kinetic parameters for supportless and carbon supported Au-Rh (3:1) catalysts at 25 °C.

Catalyst	j_d (mA/cm^2)	On set potential (V)	$E_{1/2}$ (V)	j_k (mA/cm^2)	$10^3\ k$ (cm/s)	b (mV/dec)	$10^5\ i_0$ (A/cm^2)	n	MA (mA/mg$_{Au}$)	IA or SA (A/m$^2{}_{Au}$)
Au-Rh (3:1)	4.41	0.11	-0.11	1.41	4.47	96	2.19	4.09	106	3.25
Au-Rh(3:1)/VC	3.88	0.06	-0.12	0.71	4.25	143	1.00	3.38	58	3.00

j_d- limiting current density; $E_{1/2}$- half-wave potential; j_k- kinetic current density @ -0.1 V vs. SHE; k- kinetic rate constant; i_0- exchange current density; n- number of electrons transferred; MA- mass activity @ -0.1 V vs. SHE; IA- intrinsic activity @ -0.1 V vs. SHE.

Table of Content/ Graphical Abstract

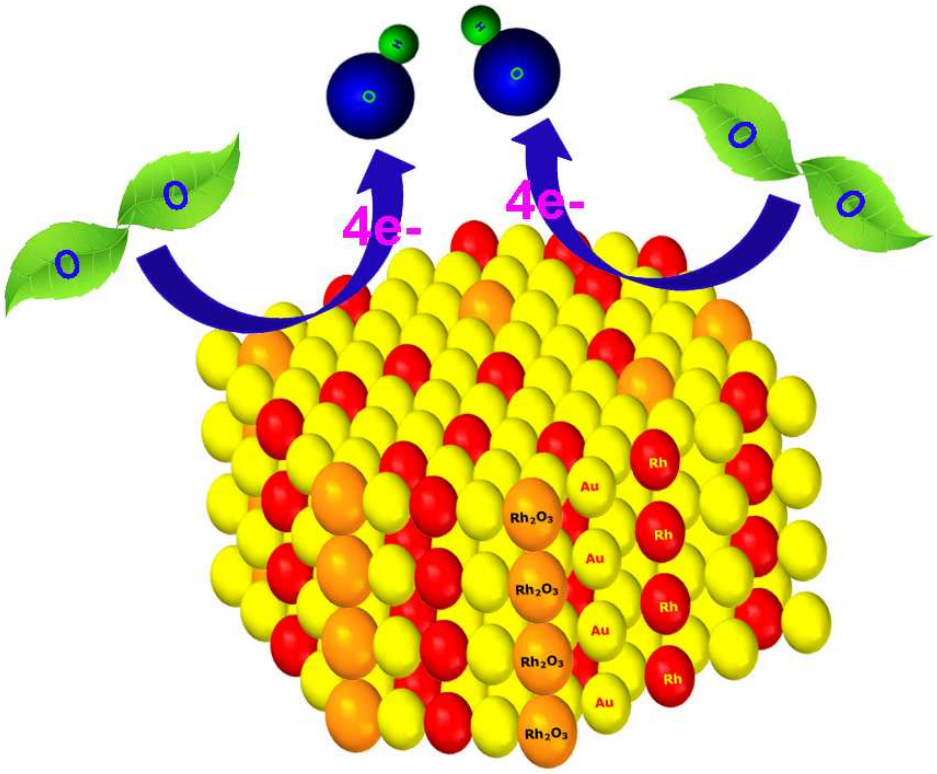

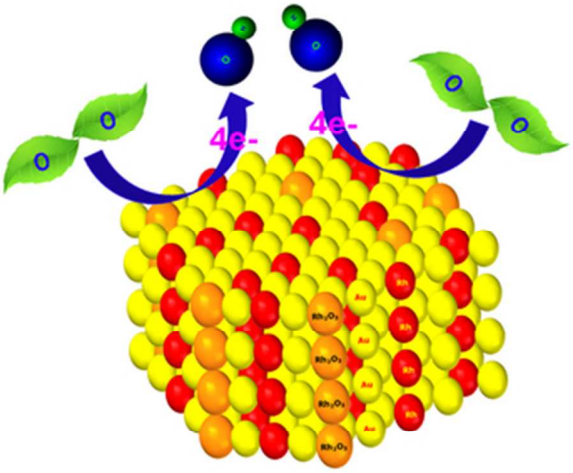

Oxygen Reduction Reaction on Au-Rh Nanoclusters

50x40mm (300 x 300 DPI)